




High performance direct absorption spectroscopy of pure and binary mixture hydrocarbon gases in the 6–11 μm range

Robert Heinrich^{1,2}  · Alexandru Popescu² · Andreas Hangauer² · Rainer Strzoda² · Sven Höfling^{1,3}

Received: 31 January 2017 / Accepted: 26 June 2017
© The Author(s) 2017. This article is an open access publication

Abstract The availability of accurate and fast hydrocarbon analyzers, capable of real-time operation while enabling feedback-loops, would lead to a paradigm change in the petro-chemical industry. Primarily gas chromatographs measure the composition of hydrocarbon process streams. Due to sophisticated gas sampling, these analyzers are limited in response time. As hydrocarbons absorb in the mid-infrared spectral range, the employment of fast spectroscopic systems is highly attractive due to significantly reduced maintenance costs and the capability to setup real-time process control. New developments in mid-infrared laser systems pave the way for the development of high-performance analyzers provided that accurate spectral models are available for multi-species detection. In order to overcome current deficiencies in the availability of spectroscopic data, we developed a laser-based setup covering the 6–11 μm wavelength range. The presented system is designated as laboratory reference system. Its spectral accuracy is at least $6.6 \times 10^{-3} \text{ cm}^{-1}$ with a precision of $3 \times 10^{-3} \text{ cm}^{-1}$. With a “per point” minimum detectable absorption of

$1.3 \times 10^{-3} \text{ cm}^{-1} \text{ Hz}^{-1/2}$ it allows us to perform systematic measurements of hydrocarbon spectra of the first 7 alkanes under conditions which are not tabulated in spectroscopic database. We exemplify the system performance with measured direct absorption spectra of methane, propane, iso-butane, and a mixture of methane and propane.

1 Introduction

Important industrial production processes in the petrochemical industry require constant and accurate monitoring. Among different other parameters, monitoring the exact composition of process streams is a crucial prerequisite, which impacts quality control, process optimization, production and energy efficiency, waste reduction, and eventually the overall profitability. Currently gas chromatographs (GCs) are widely employed, as they offer the ability to decompose the process stream while measuring the concentration of each constituent. However, GCs require sophisticated and cost-intensive measurement and calibration systems, with a delayed response [1]. The latter stems mainly from sample lines and thus inhibits real-time operations and feedback-loops. Hence, real-time measurements of multi-components in process streams, even though limited to a certain number of individual constituents, would respond to industry requirements. Furthermore, a significant amount of applications in the petrochemical industry have an apriori well-known target composition. As hydrocarbons (HCs) absorb in the mid-infrared (MIR), the employment of spectroscopic systems responding to the target composition is very attractive.

Fourier transform infrared (FTIR) spectrometers are widely used within industrial applications and research due to their broad spectral coverage and the availability of large spectral

This article is part of the topical collection “Field Laser Applications in Industry and Research” guest edited by Francesco D’Amato, Erik Kerstel, and Alan Fried.

✉ Alexandru Popescu
popescu.alexandru@siemens.com

✉ Sven Höfling
sh222@st-andrews.ac.uk

¹ Technical Physics, University of Würzburg, Am Hubland, 97074 Würzburg, Germany

² Corporate Technology, Siemens AG, Otto-Hahn-Ring 6, 81739 Munich, Germany

³ SUPA, School of Physics and Astronomy, University of St Andrews, St Andrews KY16 9SS, UK

beam splitter separating the beam at a ratio of 2:1 while the smaller fraction is coupled through an anti-reflection-coated ZnSe window and a mid-IR transparent multi-mode PIR-fiber into a high-resolution wavelength meter (HighFinesse, WS6-200 IR-3). The wavelength meter offers a high spectral precision of 100 MHz with a time resolution of 70 Hz and serves as wavelengths reference over the entire spectrum. The reflected part of the beam passes a mechanical chopper wheel. It applies an intensity modulation of 1 kHz to the beam. The reference signal from the control unit of the chopper is used to demodulate the recorded detectors signals, which results in a significant reduction of low-frequency noise. Another ZnSe beam splitter guides the beam to the gas cell and the reference detectors. The light passes a 1-cm short path gas cell through wedged ZnSe windows. The cell is temperature controlled by a high stability temperature controller. A gold-coated off-axis parabolic mirror with focal length of 25.4 mm focuses the beam on a thermoelectric cooled HgCdTe detector with $1 \times 1 \text{ mm}^2$ detector area. Another detector serves as reference monitoring the laser power and a third detector records the signal after the light passing through a slightly tilted Ge-etalon with a Free Spectral Range (FSR) of 1.46 GHz. The etalon serves as additional measurement reference. Each detector signal is amplified by a variable gain high speed current amplifier and the data are subsequently digitized with a commercial data acquisition board. The EC-QCL system and the data acquisition are fully computer controlled.

2.2 Gas sample preparation unit

Generally speaking, fluctuations in pressure and temperature as well as in the mixing ratios of the investigated gas mixtures have a strong effect on the resulting spectral characteristics [19]. Thus, it is mandatory to control the measurement conditions precisely in order to measure highly accurate reference spectra. A custom-made gas supply and mixing unit (cf. Fig. 2) was constructed in order to provide all 7 hydrocarbon gases of interest at various pressures and temperatures with an arbitrary composition. The respective gases are fed individually one after another by Mass Flow Controllers (MFCs) to a pipe system where the gas can either be led directly to the gas cell of the optical setup or through another MFC to a gas sample cylinder of 1-l volume as temporary storage. Providing real gas mixtures of known composition requires the consideration of gas-specific molecular attraction and interaction properties [20]. Especially, the larger hydrocarbons show strong deviations from ideal gas behavior [21] resulting in gas compressibilities that are depending on the overall pressure and the respective partial pressure of the other gases involved in the gas mixture. Therefore, the gas mixtures were calculated

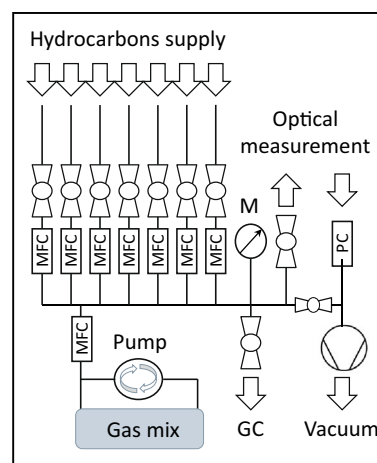


Fig. 2 Schematic of the custom made gas mixing unit and its main components: mass flow controller (MFC), sample cylinder (*Gas mix*), oil-free diaphragm pump (*Pump*), high-resolution manometer (*M*), gas chromatograph (*GC*), pressure controller (*PC*), oil-free scroll pump (*Vacuum*)

with the Peng-Robinson equation of state [22] which considers the real gas properties by an attractive pressure term that was modified to be most suitable for predicting phase and volumetric behavior of natural gas mixtures.

The mixtures are realized in the temporary storage by feeding the gases one after the other into the evacuated sample cylinder while the MFC valve is set entirely open in purge mode. The mixture preparation requires to start with the heaviest hydrocarbon and to proceed with gases of decreasing molar mass. This procedure takes the decreasing vapor pressures of the individual gases with increasing molar mass into account and increases the overall pressure of the respective mixture. Particular attention has been paid to the feeding of pentanes, as they are liquid under ambient conditions. The pentane source is cooled a few kelvin below the temperature of the storage. As the gases are filled one after the other into the sample cylinder, a layering of the components in the storage occurs which would lead to inhomogeneous gas mixtures when directly led to the spectroscopic measurement. For ensuring a homogeneous mixture of the gases, we circulate them by pumping with an oil-free diaphragm pump.

The gas pressure is monitored with a high precision manometer that possesses a precision of 1 mbar, a measurement accuracy of $\leq 0.05\%$ of its full-scale pressure and a total pressure range from 0 mbar to 10 bar (cf. Fig. 2). A high-resolution pressure controller which is placed downstream behind the gas cell controls the pressure in the gas cell while an oil-free scroll pump permits evacuation of the system up to a residual pressure of 0.01 mbar. The samples are measured with a constant mass flow through the gas cell while the pressure controller ensures a stability of

± 0.3 mbar of the setpoint. The temperature of the cell is stabilized and varies within a range of ± 0.2 K. All devices are fully computer controlled.

3 Measurement method

The employed commercial EC-QCL system offers a broad tunability of the wavelength but suffers from mode-hops caused by the fixed external cavity length of each individual laser. Littrow-type arrangements have been reported with a movable grating by a piezo-actuated translation stage for obtaining fine control of the cavity length and the grating angle leading to mode-hop-free operation [9, 23]. In our laser system, the emission is determined by the Fabry–Pérot (FP) modes from the fixed external cavity length of the grating and the back facet of the QCL chip. But also mode-hops between chip modes of the respective QCL occur. Therefore, realizing laser emission covering the entire gain spectrum of one QCL chip requires an additional modulation of the chip temperature from 17 to 23 °C alternating with a stepwise change of the cavity length. This procedure shifts the individual FP modes accordingly to the temperature change of the QCL and eventually covers the entire gain spectrum of the laser, albeit not entirely gap-less and not ordered [24, 25].

Figure 3 illustrates the measurement procedure. The grating angle is set to a specific wavelength and the chip temperature is decreased stepwise from 23 to 17 °C by 0.1 K each step which is a factory-set limitation. Before each temperature decrement, the laser current is shortly

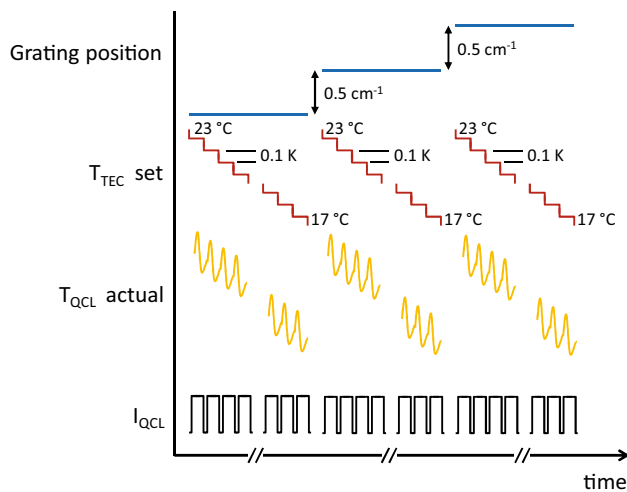


Fig. 3 Schematic illustration of the measurement procedure for 3 grating positions: stepwise set-point of the TEC temperature (T_{TEC} set), resulting QCL temperature oscillating around the set value (T_{QCL} actual), and QCL current switched on and off for every temperature step (I_{QCL}). The temperature variation leads to mode-hops and a corresponding variation in wavenumber spanning a width of 0.8 cm^{-1}

set below the gain threshold of the QCL chip. Due to the switching of the laser emission, the thermal load abruptly changes and the temperature of the QCL is oscillating around its set value due to the limited bandwidth of the employed thermoelectric cooler (TEC) (cf. Fig. 3). This leads to a tuning of the emitted mode around the central wavelength set by the grating position. After a full temperature sweep, the grating is stepwise turned and the QCL accesses the following emission mode 0.5 cm^{-1} next to its former emission mode and the temperature tuning is repeated in the same way. This procedure results in a scanning rate of $8.33 \times 10^{-4} \text{ cm}^{-1}/\text{s}$.

Figure 4 depicts measured wavelength tuning, which results from three temperature increments at a fixed grating position, together with the corresponding detector signal. The operation of the laser and the data acquisition are synchronized, and referenced by the wavelength meter. Due to the statistic behavior of mode-hops several emission modes are accessed multiple times and result in a wavelength oversampling. The collected data are sorted and stitched after the measurement.

4 Data evaluation

4.1 Demodulation and wavelength assignment

The three detector signals and the chopper reference are recorded on independent channels with a sample rate of $f_{\text{DAQ}} = 250 \text{ kS/s}$ each. A digital demodulation of the detector signals is used for noise reduction of low-frequency noise leading to a sample rate of $f_D = 20 \text{ Hz}$ for each demodulated detector value. The wavelength meter is recording independently during the whole measurement with a sample rate of $f_W = 70 \text{ Hz}$. This oversampling allows us to (1) average the wavelength values recorded

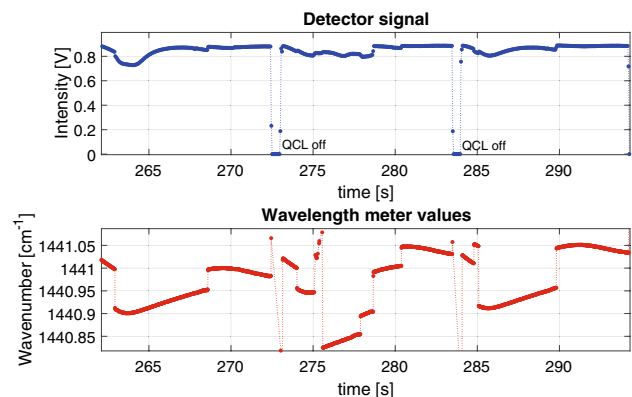


Fig. 4 Detector signal (upper graph) and corresponding wavelength meter values (lower graph) for three temperature decrements with a fixed grating position

during each demodulation of a detector value, and (2) to identify mode-hops which might occur during the demodulation of the detector signals. The criterion identifies a mode-hop, when the difference between two subsequently measured wavelength values reaches a value equal or larger than the internal mode spacing of the EC-QCL of 0.04 cm^{-1} (cf. Fig. 4). The corresponding demodulated detector signals are discarded.

4.2 Normalization

Calculating a normalized absorption spectrum from the recorded detector signals is subtle and requires more insight in the employed detectors. We employ detectors, which are designed to have a linear response up to 100 mW optical power in order to meet the dynamic range of the EC-QCL. Therefore, the wavelength-dependent responsivity is low with a maximum value of 0.03 A/W . This leads to an incomplete absorption of the incident light for high powers. Due to the coherent laser source etaloning of the light in the detector chip substrate occurs and a wavelength-dependent intensity modulation of the signal is inevitable. Due to tolerances, the fringe pattern on each detector is phase-shifted with respect to each other and they do not compensate when directly dividing one detector signal with the other. However, due to the constant phase shift, which leads to a frequency beat with a periodicity of 4.5 cm^{-1} , it is possible to correct this modulation of the signal by measuring the background $I(\nu_i)_{\text{bkg}}/I(\nu_i)_{\text{ref,bkg}}$ of the gas cell, while being purged with dry nitrogen. A coarse tuning of the grating over the respective wavelength region with a spectral resolution of 0.5 cm^{-1} is fully sufficient.

As described in Sect. 3, the fine tuning of the EC-QCL emission wavelength is achieved by the stepwise temperature tuning of the QCL. The resulting intensity modulation (cf. Fig. 4) is then compensated by the reference detector (cf. Fig. 2) via $I(\nu_i)_{\text{abs}}/I(\nu_i)_{\text{ref,abs}}$ and results in the following transmission signal $T(\nu)$:

$$T(\nu_i) = \frac{I(\nu_i)_{\text{abs}}}{I(\nu_i)_{\text{ref,abs}}} \cdot \left(\frac{I(\nu_i)_{\text{bkg}}}{I(\nu_i)_{\text{ref,bkg}}} \right)^{-1} \quad (1)$$

4.3 Data rejection

Multi-mode emission, that arises from occasional back-reflections into the laser, distorts the recorded signal. These reflections are well suppressed by exact alignment of the optical system but occasionally occur for wide spectral sweeps as the alignment is wavelength dependent. In a first step, applying a median filter to the normalized data effectively removes obvious outliers in the transmission spectrum.

In a second step, we investigate the Etalon spectrum as subsequent filtering criterion. The Airy transmission function

$$T(\nu) = \frac{T_{\text{max}}}{1 + (2F/\pi)^2 \sin^2(\pi\nu/\nu_F)} \quad (2)$$

is fitted to the Etalon spectrum (cf. Fig. 5) with the following free parameters: T_{max} denotes the maximum transmission and is used for normalization, F the finesse of the etalon and ν_F the free spectral range. Data values that deviate a threshold of $\tau \geq 5\%$ from the determined Etalon-fit are discarded from the data set. This allows us to filter values that strongly deviate even when the median filter fails. For clarity, we omit discussing the Etalon interference and the parameter results in more detail, as it would not contribute to the purpose of the sensitivity estimation and the data rejection procedure.

4.4 Sensitivity estimation

Due to the limited knowledge in accurate line parameters and absorption cross sections for the targeted $\text{C}_1\text{--C}_5$ hydrocarbons, we cannot compare the measured spectra to numerically modeled spectra in order to determine the sensitivity of the presented reference system. Hence, we estimate the sensitivity of our measurements by a comparison of the measured etalon transmission with a fit of the Airy function to the data. The upper graph of Fig. 5 depicts a fit of the Airy function to the measured Etalon data and the lower graph depicts their residual. By calculating the square deviation of each transmission value from the Airy fit and subsequent averaging, we obtain a mean square error of $\text{MSE} = 0.59\%$. It is reasonable to assign the deviation of the etalon transmission to the

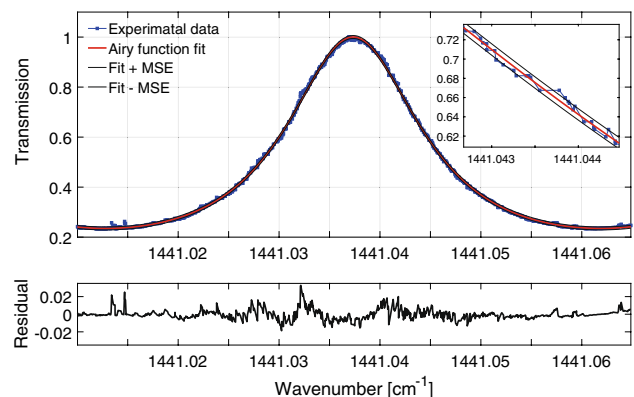


Fig. 5 Upper graph normalized Etalon transmission and numerical fit of Eq. (1) to the data; Lower graph residual of the experimental data and the numerical fit

gas transmission measurements as well, and according to the metrics discussed by Moyer et al. [26] we can thus calculate a “per point” minimum detectable absorption (MDA_{pp}) for comparing our instrument to common instrument sensitivity data via

$$MDA_{pp} = \frac{\Delta P}{P} \cdot \frac{1}{\sqrt{BW}}. \quad (3)$$

The term $\Delta P/P$ describes the limiting noise level ΔP of a measurement normalized by the total power P while BW corresponds to the sampling bandwidth that is given by the demodulation in our measurements. Accordingly, we insert the calculated MSE for $\Delta P/P$ and 20 Hz for the bandwidth BW . This leads to a value of $MDA_{pp} = 1.3 \times 10^{-3} \text{ Hz}^{-1/2}$ as minimum detectable absorption for our measurement system. This value compares well with other broadband spectroscopic techniques (cf. Table 5 in Ref. [3] and discussion therein).

5 Results and discussion

Presenting spectra for all available gases, the large number of their possible mixtures as well as the wide range of pressure and temperature we can adjust in our setup would be beyond the scope of this paper.

In order to illustrate the measurement performance of the system by selected example measurements, we present spectra of a pure iso-butane, methane, propane and a spectrum of a 1:1 mixture of methane and propane. For clarity, the presented spectra are plotted on a constant grid of 0.001 cm^{-1} which means that the raw data points were averaged over constant wavenumber bins of 0.001 cm^{-1} width. An exception is depicted in Fig. 7, which exemplifies also the raw data.

5.1 Pure gas reference spectrum

Iso-butane is documented in the PNNL database for a spectral range from 6500 to 600 cm^{-1} . These measurements were acquired for different partial pressures of the individual species while an overall pressure of 1 bar was adjusted by adding high-purity nitrogen. The resolution of the database spectra is limited to 0.112 cm^{-1} by the maximum displacement of the used FTIR [16].

Figure 6 shows the measured transmission spectrum of iso-butane in the spectral range from 1462 to 1464 cm^{-1} and compares the data to a curve from the PNNL database. For comparison purposes, the PNNL spectrum was adjusted to the measurement temperature and pressure of 323 K and 100 mbar, respectively, by scaling the tabulated cross section according to the gas density of our measurement.

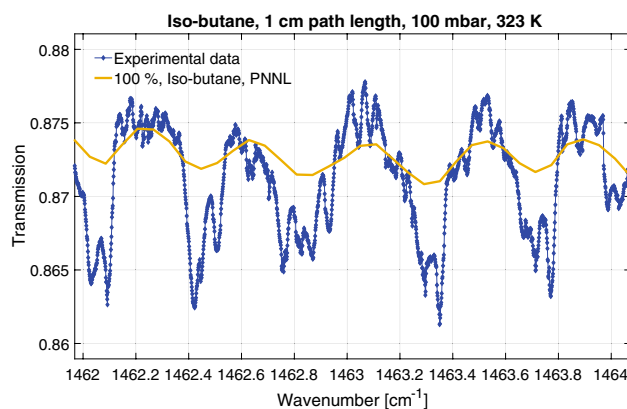


Fig. 6 Measured transmission spectrum of iso-butane and respective scaled PNNL spectrum for a temperature and pressure of 323 K and 100 mbar, respectively. The structure of the measured curve demonstrates the increase in resolution of the measurements compared to the database. The scaling of the PNNL data does not consider pressure broadening effects

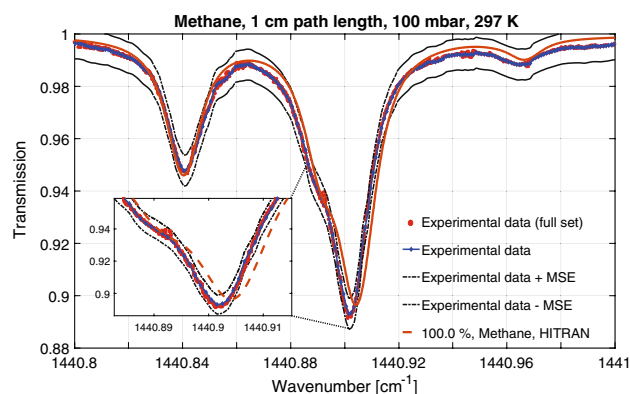


Fig. 7 Measured transmission spectrum of methane with a simulated HITRAN spectrum for a temperature and pressure of 297 K and 100 mbar, respectively. The full set of the experimental data (red) and the plot on a constant wavenumber grid (blue) emphasize the equivalence between both representations. At 1440.9 cm^{-1} small deviations between measured and simulated data become visible

The experimental data exhibit much more structure, when compared to the spectrum from the database, and reveal a multitude of overlapping narrow absorption lines. The maximum modulation depth is about four times higher than that of the PNNL spectrum and varies over 1.6% of transmission. It emphasizes the requirement for measuring the spectra of the considered hydrocarbons at low pressures as the database spectra can not be used to model spectra of C_1 – C_5 HCs at these conditions due to their acquisition at 1 bar which induces a strong broadening of the individual absorption lines. This fact gains rather more importance,

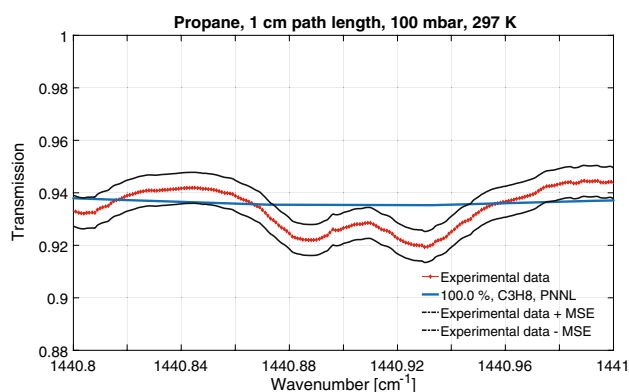


Fig. 8 Measured transmission spectrum of propane with a scaled PNNL spectrum for a temperature and pressure of 297 K and 100 mbar, respectively

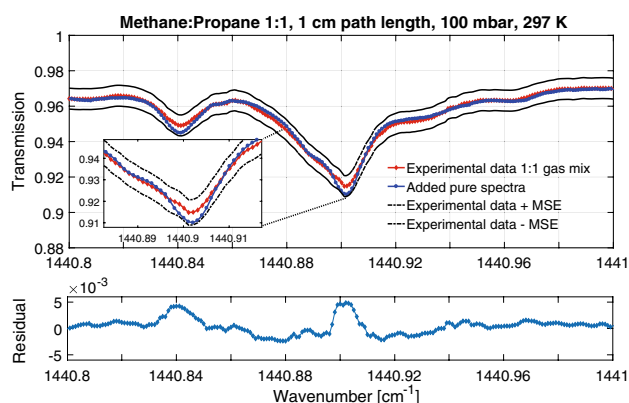


Fig. 9 Upper graph comparison of measured spectrum from 1:1 gas mixture of methane and propane at 100 mbar and 297 K with a calculated spectrum from the transmission measurements of pure gases. The inset illustrates the deviation of the transmission at the peaks of the spectra. Lower graph residual between measured and calculated spectrum

when comparing spectra of HC gas mixtures with spectra of the respective pure gases.

5.2 Spectrum of a gas mixture

In particular when it comes to multi-species detection, gas mixtures and the resulting effects on the spectral features have to be taken into consideration [19]. Our investigations start with binary mixtures, proceed to ternary and more complex mixtures. In order to exemplify the importance of this approach, we discuss in this section spectra of pure methane, pure propane and their mixture with a concentration ratio of 1:1 which were all measured at 100 mbar and 297 K, cf. Figs. 7, 8, and 9, respectively.

Figure 7 depicts the measured methane spectrum with 7 significant peaks in the range from 1440.8 to 1441 cm^{-1}

together with a simulated methane spectrum based on the HITRAN database [15]. The simulated methane spectrum was calculated with a Voigt profile and the spectral line shape parameters were scaled for the set pressure and temperature.

Generally speaking, the spectra show a general correspondence between measurement and reference, but also some small deviations are visible. Obviously, the main peak at 1440.9 cm^{-1} is shifted compared to the reference measurement by 0.0026 cm^{-1} and 0.33% in transmission. Concurrently, the second prominent peak at 1440.84 cm^{-1} better coincides with the reference spectrum in wavelength as well as in transmission (difference 0.0001 cm^{-1} , 0.19%). Thus, we can exclude a systematic shift on our measurements in wavelength as in transmission.

For a further quantitative analysis of this deviations, we want to compare precision and accuracy of the wavelength meter with our measurement results. The wavelength meter measures over a broad range of 2–11 μm with a guaranteed precision of 100 MHz or 0.003 cm^{-1} , and an accuracy of 200 MHz within the full spectral coverage. A regular one point calibration with a reference laser system (High-Finesse, SLR-1532) locked to an acetylene absorption line with a nominal output of 1.532 $\mu\text{m} \pm 0.07 \text{ pm}$ provides stable measurement conditions. Although the peak deviations are within the error margin of the device, we can determine from the etalon transmission signal an average spectral sampling of $1 \times 10^{-4} \text{ cm}^{-1}$, consequently a resolution that is 30 times higher than the device precision specification. By comparing these values, we can conclude that the latter is a rather conservative estimation valid for the whole device measurement range of 9 μm . This interpretation is also fostered by the match of the other methane line in Fig. 7.

A preliminary conclusion is that the deviations between the HITRAN and the measured data are considerably low since they are covered by the precision limit of the measurement system. But as a systematic shift on the data could be disproved, further reference measurements have to be conducted that should reveal if the deviations are stable and thus either represent a characteristic of the measurement system or demonstrate an inaccuracy of the database.

The measured propane spectrum, depicted in Fig. 8, demonstrates again the limited spectral resolution of the PNNL database compared to our setup.

As measuring not just the pure spectra of the hydrocarbons but also absorption of their respective mixtures is within the objectives of our investigations, we present a measurement of a methane and propane mixture with a concentration of 50% for each gas. We mentioned in Sect. 2.2 that the ratios of gas mixtures and their respective components can have effects on molecular spectra due to collisional effects [19]. An extensive description of these effects in spectra of hydrocarbon mixtures would be

beyond the scope of this report. But in order to obtain an evidence if collisional effects affect our measurements, we have compared the spectrum of the gas mixture with two measurements of the pure gases. Therefore, we calculated the sum of the pure spectra according to the absorption law by Lambert-Beer:

$$I_{100\%}(\lambda) = I_0 \cdot e^{-\alpha(\lambda)cd} \quad (4)$$

with λ the wavelength or wavenumber, I_0 the incident intensity, α the absorption coefficient of the respective gas species, c the gas concentration and d the length of the optical path through the gas sample. In the reference measurements, the individual gases had a concentration c of 100% thus yielding a respective intensity of transmission $I_{100\%}(\lambda)$. For calculating the intensity of a mixture with half of the respective gas concentration $c/2$, we have to take the logarithm of the individual transmission signal of methane and propane, divide each by 2, and insert the sum in the law of Lambert-Beer:

$$I_{1:1}(\nu) = e^{(\ln(I_{\text{CH}_4})/2 + \ln(I_{\text{C}_3\text{H}_8})/2)}. \quad (5)$$

The calculated intensity $I_{1:1}(\nu)$ can then be compared to the measured signal of the gas mixture.

Figure 9 shows the transmission measurement of the gas mixture in red and the calculated spectrum from the pure spectra in blue. The residual of both spectra is depicted in the graph below. It is visible from the spectra that the binary mixture causes no significant change of line shape or shift of the peak position compared to the pure spectra within the instruments' accuracy.

Further investigations should be dedicated to reveal if the deviation in both peaks (see residual in Fig. 9) result is a physical effect that varies with pressure, temperature, concentration of the respective gas and the individual components of the mixture.

6 Conclusion

A measurement setup based on a commercial EC-QCL system was developed and assessed regarding its capability to measure direct absorption spectra of hydrocarbons and their mixtures. The measurements of the pure hydrocarbons spectra were compared to available database spectra. We demonstrate (1) a measurement procedure that yields a gapless wavelength coverage in the spectral range from 6 to 11 μm . The overall spectral accuracy is delimited by the guaranteed accuracy of the employed wavelength meter. From the etalon spectrum we extract a far better frequency sampling of $1 \times 10^{-4} \text{ cm}^{-1}$; (2) a "per point" minimum detectable absorption of $\text{MDA}_{\text{pp}} = 1.3 \times 10^{-3} \text{ Hz}^{-1/2}$, that is in the same range or better than recently reviewed other techniques for gas-phase broadband spectroscopy [3]; (3)

a measurement system that provides stable measurement conditions and the capability to prepare gas samples of the first 7 hydrocarbons either as pure gases or mixtures; (4) the measurement of pure gases and a binary gas mixture.

The chosen approach combines high spectral resolution and high sensitivity with a wide spectral range. Hence, the developed system is well suited to measure the required reference spectra of C_1 – C_5 hydrocarbons and their mixtures providing yet unavailable fundamentals for laser-based spectroscopic process control systems for the petro-chemical industry. The latter is of outstanding importance, as line broadening effects due to the mixture of gases have to be considered for proper data evaluation. Even though the presented data provide a first hint towards these broadening effects, their influence can be studied by improving the system with larger gas cells providing longer absorption path length. Increasing the cell length from 1 to 10 cm would deliver the same factor in absorbance and thus reveal the interaction effects of hydrocarbons mixtures with more detail.

Acknowledgements We gratefully thank Dr. Frank Olschewski for supporting the simulation of real gases. The project has received funding from the European Unions Horizon 2020 research and innovation program under Grant Agreement No. 636930.

Open Access This article is distributed under the terms of the Creative Commons Attribution 4.0 International License (<http://creativecommons.org/licenses/by/4.0/>), which permits unrestricted use, distribution, and reproduction in any medium, provided you give appropriate credit to the original author(s) and the source, provide a link to the Creative Commons license, and indicate if changes were made.

References

1. G.A. Eiceman, H.H. Hill Jr., J. Gardea-Torresdey, Gas chromatography. *Anal. Chem.* **70**(12), 321R–339R (1998)
2. Jane Hodgkinson, Ralph P. Tatam, Optical gas sensing: a review. *Meas. Sci. Technol.* **24**(1), 012004 (2013)
3. Kevin C. Cossel, Eleanor M. Waxman, Ian A. Finneran, Geoffrey A. Blake, Jun Ye, Nathan R. Newbury, Gas-phase broadband spectroscopy using active sources: progress, status, and applications. *J. Opt. Soc. Am. B* **34**(1), 104–129 (2017)
4. Jerome Faist, Federico Capasso, Deborah L. Sivco, Carlo Sirtori, Albert L. Hutchinson, Alfred Y. Cho, Quantum cascade laser. *Science* **264**(5158), 553–556 (1994)
5. R.Q. Yang, Infrared laser based on intersubband transitions in quantum wells. *Superlattices Microstruct.* **17**, 77–77 (1995)
6. Chuan Peng, Guipeng Luo, Q.Le Han, Broadband, continuous, and fine-tune properties of external-cavity thermoelectric-stabilized mid-infrared quantum-cascade lasers. *Appl. Opt.* **42**(24), 4877–4882 (2003)
7. Richard Maulini, Mattias Beck, Jrme Faist, Emilio Gini, Broadband tuning of external cavity bound-to-continuum quantum-cascade lasers. *Appl. Phys. Lett.* **84**(10), 1659–1661 (2004)
8. N. Bandyopadhyay, M. Chen, S. Sengupta, S. Slivken, M. Razeghi, Ultra-broadband quantum cascade laser, tunable over

- 760 cm^{-1} , with balanced gain. *Opt. Express* **23**(16), 21159–21164 (2015)
9. G. Wysocki, R. Lewicki, R.F. Curl, F.K. Tittel, L. Diehl, F. Capasso, M. Troccoli, G. Hoffer, D. Bour, S. Corzine, R. Maulini, M. Giovannini, J. Faist, Widely tunable mode-hop free external cavity quantum cascade lasers for high resolution spectroscopy and chemical sensing. *Appl. Phys. B* **92**(3), 305–311 (2008)
 10. T. Tsai, G. Wysocki, External-cavity quantum cascade lasers with fast wavelength scanning. *Appl. Phys. B* **100**(2), 243–251 (2010)
 11. Brian E. Brumfield, Matthew S. Taubman, Jonathan D. Suter, Mark C. Phillips, Characterization of a swept external cavity quantum cascade laser for rapid broadband spectroscopy and sensing. *Opt. Express* **23**(20), 25553–25569 (2015)
 12. B.E. Brumfield, M.S. Taubman, M.C. Phillips, Rapid and sensitive quantification of isotopic mixtures using a rapidly-swept external cavity quantum cascade laser. *Photonics* **3**(2), 33 (2016)
 13. R. Ostendorf, L. Butschek, S. Hugger, F. Fuchs, Q. Yang, J. Jarvis, C. Schilling, M. Rattunde, A. Merten, J. Grahmann, D. Boskovic, T. Tybussek, K. Rieblinger, J. Wagner. Recent advances and applications of external cavity-QCLs towards hyperspectral imaging for standoff detection and real-time spectroscopic sensing of chemicals. *Photonics* **3**(2), 28 (2016)
 14. R. Ostendorf, L. Butschek, A. Merten, J. Grahmann, J. Jarvis, S. Hugger, F. Fuchs, J. Wagner. Real-time spectroscopic sensing using a widely tunable external cavity-QCL with MOEMS diffraction grating. *Proc. SPIE*, 9755:975507–975507–8 (2016)
 15. L.S. Rothman, I.E. Gordon, Y. Babikov, A. Barbe, D. Chris Benner, P.F. Bernath, M. Birk, L. Bizzocchi, V. Boudon, L.R. Brown, A. Campargue, K. Chance, E.A. Cohen, L.H. Coudert, V.M. Devi, B.J. Drouin, A. Fayt, J.-M. Flaud, R.R. Gamache, J.J. Harrison, J.-M. Hartmann, C. Hill, J.T. Hodges, D. Jacquemart, A. Jolly, J. Lamouroux, R.J. Le Roy, G. Li, D.A. Long, O.M. Lyulin, C.J. Mackie, S.T. Massie, S. Mikhailenko, H.S.P. Miller, O.V. Naumenko, A.V. Nikitin, J. Orphal, V. Perevalov, A. Perrin, E.R. Polovtseva, C. Richard, M.A.H. Smith, E. Starikova, K. Sung, S. Tashkun, J. Tennyson, G.C. Toon, V.I. Tyuterev, G. Wagner, The HITRAN2012 molecular spectroscopic database. *J. Quant. Spectrosc. Radiat. Transf.* **130**, 4–50 (2013). (HITRAN2012 special issue)
 16. T.J. Johnson, R.L. Sams, S.W. Sharpe, The PNNL quantitative infrared database for gas-phase sensing: a spectral library for environmental, hazmat, and public safety standoff detection. in *Proc. SPIE, Chemical and Biological Point Sensors for Homeland Defense*, ed. by A.J. Sedlacek, III, R. Colton, T. Vo-Dinh, vol. 5269 (SPIE, USA, 2004), pp. 159–167
 17. L.S. Rothman, I.E. Gordon, R.J. Barber, H. Dothe, R.R. Gamache, A. Goldman, V.I. Perevalov, S.A. Tashkun, J. Tennyson, HITEMP, the high-temperature molecular spectroscopic database. *J. Quant. Spectrosc. Radiat. Transf.* **111**(15), 2139–2150 (2010)
 18. N. Jacquinet-Husson, L. Crepeau, R. Armante, C. Boutammine, A. Chédin, N.A. Scott, C. Crevoisier, V. Capelle, C. Boone, N. Poulet-Crovisier et al., The 2009 edition of the GEISA spectroscopic database. *J. Quant. Spectrosc. Radiat. Transf.* **112**(15), 2395–2445 (2011)
 19. J.-M. Hartmann, C. Boulet, D. Robert (eds.), *Collisional Effects on Molecular Spectra* (Elsevier, Amsterdam, 2008)
 20. B.E. Poling, J.M. Prausnitz, J.P. O'connell, et al., *The Properties of Gases and Liquids*, vol. 5 (McGraw-Hill, New York, 2001)
 21. K.E. Starling, J.L. Savidge, *Compressibility Factors of Natural Gas and Other Related Hydrocarbon Gases* (AGA, American Gas Association, Washington, DC, 1994)
 22. Ding-Yu. Peng, Donald B. Robinson, A new two-constant equation of state. *Ind. Eng. Chem. Fundam.* **15**(1), 59–64 (1976)
 23. Gerard Wysocki, Robert F. Curl, Frank K. Tittel, Richard Maulini, Jean-Marc Bulliard, Jérôme Faist, Widely tunable mode-hop free external cavity quantum cascade laser for high resolution spectroscopic applications. *Appl. Phys. B* **81**(6), 769–777 (2005)
 24. P. Buerki, M. Weida, CW tuning behavior of CW-PLS lasers. Technical report, Daylight Solutions, Inc. (2010)
 25. G. Douberly, Application note: vintinuous tuning of a daylight solutions 6.05 CW EC-qcl without loss of coverage due to mode hops via sequential scans at different laser head temperatures. Technical report, Department of Chemistry, University of Georgia (2010)
 26. E.J. Moyer, D.S. Sayres, G.S. Engel, J.M. St. Clair, F.N. Keutsch, N.T. Allen, J.H. Kroll, J.G. Anderson, Design considerations in high-sensitivity off-axis integrated cavity output spectroscopy. *Appl. Phys. B* **92**(3), 467 (2008)